Electrical, Optical and Structural Properties of $Cu_2Zn_{0.8}Cd_{0.2}SnS_4$ Quinternary Alloy Nanostructures Synthesized by Spin Coating Technique

A. S. Ibraheam[1], Y. Al-Douri[1,2,*], Abubaker S. Mohammed[3], Deo Prakash[4] , U. Hashim[1], K.D. Verma[5]

[1]Institute of Nano Electronic Engineering, University Malaysia Perlis, 01000 Kangar, Perlis, Malaysia
[2]Physics Department, Faculty of Science, University of Sidi-Bel-Abbes, 22000-Algeria
[3]Department of Physics, College of Education for Pure Science, University of Anbar, Ramadi, Iraq
[4]School of Computer Science & Engineering, Faculty of Engineering, SMVD University, Kakryal, Katra-182320, J&K, India
[5]Material Science Research Laboratory, Department of Physics, S. V. College, Aligarh –202001, U.P., India
[*]E-mail: yaldouri@yahoo.com

$Cu_2Zn_{0.8}Cd_{0.2}SnS_4$ quinternary alloy nanostructures with different Cu concentration (0.3, 0.5, 0.7 and 0.9 mol/L) were grown on glass substrate, using the spin coating technique. The structural and morphological studies were carried out by X-ray diffraction (XRD), Field Emission-Scanning Electron Microscope (FE-SEM) and Atomic Force Microscopy (AFM) techniques. Optical studies, carried out through UV-visible (UV-vis) spectrophotometer revealed that the direct band gap energy of $Cu_2Zn_{0.8}Cd_{0.2}SnS_4$ quinternary alloy nanostructures decreases as Cu concentration increases. The transmittance value in the range 63-49% was also dependent on Cu concentration. The refractive index and optical dielectric constant gave good agreement with experimental and theoretical results. Electrical properties studied by Hall Effect measurement, showed p-type conductivity, with a carrier concentration between 7.819×10^{12} cm^{-3} and 3.76×10^{14} cm^{-3}.

1. INTRODUCTION

While $CuIn_{1-x}Ga_xSe_2$ (CIGS) has attracted much attention due to its stability and high power conversion efficiency [1-3], further development in the field of thin-film solar cells keeps being impeded. After a lot of effort had been made in order to find low-cost, non-toxic, and earth-abundant

elements for thin-film solar cells, Cu_2CdSnS_4 (CCTS) and Cu_2ZnSnS_4 (CZTS), were considered as materials, that might substitute CIGS due to their direct band gap, E_g=1.4-1.5 eV with high absorption coefficient of 10^4 cm^{-1}, p-type conductivity, and their being earth-abundant [4].

Therefore, utilization of CZTS as absorbent for solar cells might reduce the problems related to the resource saving and environmental pollution [5]. Moreover, numbers of experiment have been conducted to prepare CZTS thin films, through pulsed laser deposition technique [6], fast co-evaporation [7], sputtering-sulfurization method [8], sputtering [9], thermal evaporation [10], electrodeposition [11,12], spray pyrolysis [13] and hot injection method [14].

Sulphur incorporation at the precursor stage on the growth of CZTS was studied by Chalapathi et al. [15]. Where, the thin films have been prepared in a two-stages process. The elemental composition, structural, microstructural and optical properties of these films were analyzed and it was discovered that the lattice parameters were a=0.542 nm and c=1.089 nm. Additionally, at 550 °C for 30 min, distinct and compact grain size of CZTS was obtained with a grain size range of 400-800. A direct band gap between 1.44 eV and 1.56 eV (depending on the annealing temperature and duration) was as well discovered. Furthermore, Dasgupta et al. [16] have also successfully produced *pn*-junction devices based on layers of Cu_2ZnSnS_4 (CZTS) and (AgInS$_2$@Cu) ternary nanocrystals. From the capacitance–voltage characteristics of the *pn*-junctions, they have evaluated the width of the depletion region that extended to the two layers separately. By forming such a device, they could eliminate the sections of the *p-* and the *n*-layers, that would otherwise have increased the internal resistance of the solar cells without contributing to short-circuit current. While, Huang et al. [17] have demonstrated that starting from first principles density functional theory, the carrier mobility in CZTS NC–ligand complex can be determined quantitatively, and guided by specific model, they have developed a low-cost, low-temperature technique to fabricate CZTS thin films which have a carrier mobility of up to 10.9 cm^2/(VS).

The current work aims primarily to study the effect of copper (Cu) concentration on the structural, morphological, optical and electrical properties of $Cu_2Zn_{0.8}Cd_{0.2}SnS_4$ quinternary alloy nanostructures (prepared by spin coating), through XRD, FE-SEM, AFM, UV-vis and Hall effect measurement.

2. EXPERIMENTAL

The analytical grade chemicals were obtained from Sigma-Aldrich Company. The $Cu_2Zn_{0.8}Cd_{0.2}SnS_4$ quinternary alloy nanostructures were deposited on a glass substrate, using the spin coating technique, which includes following steps:

The solution of $Cu_2Zn_{0.8}Cd_{0.2}SnS_4$ precursors were prepared from copper (II) chloride monohydrate (0.3, 0.5, 0.7 and 0.9 mol/L), zinc (II) acetate dihydrate (0.3 mol/L), tin (II) chloride dihydrate (0.3), cadmium (II) chloride (0.3 mol/L), thiourea (0.3 mol/L), 2-methoxyethanol and monoethanolamine (MEA). The solvent and stabilizer were the 2-metho and MEA, respectively. In order to dissolve the salts, the solution was stirred at 50 °C. The milky solution turned into yellow during the stirring. Afterwards, the solution was dropped onto the 2500 rpm rotating glass substrate for 30 seconds.

After the spin coating deposition, the films were dried at 250 °C for 80 min on a hot plate. The coating and drying processes were repeated for seven times to obtain the required thickness.

$$Molarity (M) = \frac{M_s}{V} \tag{1}$$

$$M_s = \frac{W(gm)}{M_{wt}(grams/moles)}$$

where M_s is number of moles, V is liquid size (liter), W is weight (gm) and M_{wt} is molecular weight (gm/mol).

X-ray diffraction (XRD) system (Philips PW 1710 X-ray diffractometer, USA) with Cu Kα radiation (λ=1.54Å) was utilized in order to examine the crystal structures of $Cu_2Zn_{0.8}Cd_{0.2}SnS_4$ quinternary alloy nanostructures at different Cu concentrations. UV-visible (UV-vis) spectrophotometer (Perkin Elmer Lambda 950, USA) was used for measuring the optical properties at room temperature. Surface morphologies of $Cu_2Zn_{0.8}Cd_{0.2}SnS_4$ nanostructures were characterized by employing Field Emission-Scanning Electron Microscope (FE-SEM) system (NOVA NANO SEM 450, USA) and Atomic Force Microscope (AFM) (SII Sciko Instrument INC, SPI 3800N Probe, USA). Hall Effect measurement system with Van der Pauw configuration was employed to characterize the electrical properties and carrier concentrations of the films.

3. RESULTS AND DISCUSSION

3.1 Structural properties

The X-ray diffraction (XRD) patterns of $Cu_2Zn_{0.8}Cd_{0.2}SnS_4$ quinternary alloy nanostructures with different Cu concentrations, i.e. 0.3, 0.5, 0.7 and 0.9 M are shown in Fig. 1.The diffraction peaks at 2θ = 28.43, 30.51, 45.70, 50.43, 55.80 were attributed to the diffraction planes (112), (101), (110), (151) and (312), respectively. Preferential (112) and (312) planes of CZTS were observed for all deposited films that have the tetragonal structure of the kesterite phase. In addition, formation of secondary phases, such as ZnS, SnS and Cu_2S were also noticed. The intensity of (112), (312) and (110) peak becomes more intense and sharp, with increasing Cu concentration which evidences that the films being Cu-rich. Lattice constants a and c were investigated and calculated from XRD data corresponding to the (112) plane as given in Table 1.

$$(1/d^2) = (h^2 + k^2)/a^2) + (l^2/c^2) \tag{2}$$

where hkl is Miller indices, a and c are lattice constants and the interplane distance (d) can be calculated for all sets of $Cu_2Zn_{0.8}Cd_{0.2}SnS_4$ nanostructures using Bragg's equation [18]:

$$d = h\lambda/2\sin\theta \tag{3}$$

where λ is the wavelength of X- ray (λ=1.5406 Å) and and θ is Bragg's angle [18].

The crystalline size (D) was calculated via Scherrer's formula [18]

$$D = k\lambda/\beta\cos\theta \tag{4}$$

where k is a constant equals 0.94 and β is the Full Width at Half Maximum (FWHM). When Cu is increased from 0.3 to 0.9 mol/L, there is a gradual increase in the particle size. The $Cu_2Zn_{0.8}Cd_{0.2}SnS_4$

nanostructures deposited at 0.9 mol/L exhibited a large crystallite size of around 68 nm, indicating an enhancement of particle growth under Cu-rich conditions.

In addition, the dislocation density (δ) and strain (ε) were determined [18]:

$$\delta = 1 / D^2_{hkl} \tag{5}$$

$$\varepsilon = \beta \cos\theta / 4 \tag{6}$$

These parameters are given in Table 1. The dislocation density and strain are decreased with increasing of Cu concentration, where the highest dislocation density and strain are 7.917 x 10^{14} and 0.1038 x 10^{-3}, respectively, while the particle size and lattice constants are increased as Cu concentration increases.

Material stiffness is important in different industries, which is reflected in bulk modulus [19-24]. Many attempts have been made to explore solid's thermodynamic properties. In context of this study, thermodynamic properties, including, inter-atomic separation and bulk modulus of solids have been examined with different approximations and best-fit relations [21-25]. Additionally, more empirical approaches have been developed to accurately compute the structural and electronic properties of the solids; despite *ab initio* calculations which are very complex and require numerous efforts [25,26]. Although, the empirical methods gives applicability advantage to a broad class of materials and illustrate the trends in many cases, but, it might not be extremely accurate for each specific material.

Cohen et al. [27] established an empirical formula to for calculating the bulk modulus B_0. This formula was based on the nearest-neighbor distance, and presented good consistency of the result with the experimental data. At the same tone, an analytical expression for the bulk modulus from the total energy has been derived by Lam et al. [28], which was structurally different from the empirical formula, yet offered the same numerical results. In addition, they have obtained an analytical expression of the bulk modulus.Additionally, another concept based on the lattice constant have been established [29], where, the obtained results are consistent with the experimental data and other calculations. The two interesting features of this formula are; only the lattice constant is required as input and the computation of B_0 is trivial.

The possibility of bulk modulus to be related to the lattice constant, despite its being a qualitative concept is the main objective. It was advocated that the dominant effect is the degree of covalence, which was characterized by the Phillips' homopolar gap E_h [25]. The reason to include these data in present work is that the validity of the calculations is not restricted in computed space. Thus, it is believed that the data will be proven valuable for future work in this field.

The study of B_0 is important here as the clear differences between the lattice constant for $Cu_2Zn_{0.8}Cd_{0.2}SnS_4$ quinternary alloy nanostructures is seen in Table 1. Here, B_0 was calculated using the following empirical formula [29]:

$$B_0 = [3000 - 100\lambda] \left(\frac{a}{2} \right)^{-3.5} \tag{7}$$

where, a is the lattice constant (in Å); λ is an empirical parameter for the effect of ionicity ($\lambda = 0$; 1, 2 for group IV, III–V and II–VI semiconductors, respectively). The calculated values of B_0 are indicated In Table 1. Here it can be concluded that the present bulk modulus, which was calculated by a different way than the definition of Cohen, exhibit the same chemical trends. It is observed that Cu

concentration is proportion directly with the stiffness of $Cu_2Zn_{0.8}Cd_{0.2}SnS_4$ quinternary alloy nanostructures.

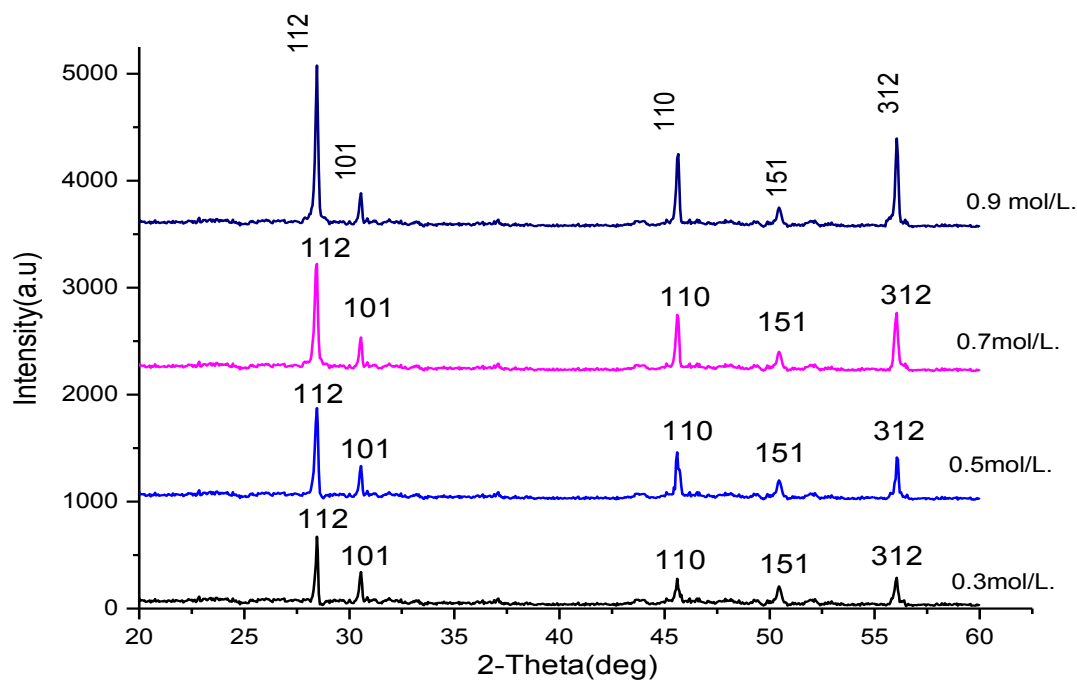**Figure 1.** XRD patterns of $Cu_2Zn_{0.8}Cd_{0.2}SnS_4$ quinternary alloy nanostructures for different Cu concentrations 0.3, 0.5, 0.7 and 0.9 Mol/L.

Table 1. Structural characteristics of $Cu_2Zn_{0.8}Cd_{0.2}SnS_4$ quinternary alloy nanostructures for different mol/L, derived from XRD results.

Molar concentration (mol/L)	Peak (θ)	d_{hkl} (002) (Å)	Particle size (nm)	Dislocation density (δ) (10^{14}) (lines/m^2)	Strain (ε) (10^{-3})	Lattice constants (Å)	Bulk modulus (B_0) (GPa)
0.3	28.43°	3.127	35.54	7.917	0.1038	a=5.440 c=10.860	84.36
0.5	28.40°	3.135	53	3.559	0.1021	a= 5.423 c= 10.851	85.29
0.7	28.39°	3.139	57	3.077	0.0754	a= 5.434 c= 10.842	84.69
0.9	28.37°	3.143	68	2.162	0.0437	a= 5.440 c= 10.821	84.36

The morphology of $Cu_2Zn_{0.8}Cd_{0.2}SnS_4$ nanostructures at different Cu concentrations have been characterized through FE-SEM, as shown in Fig. 2. Figure 2 (a) and (b) display the layers which uniformly cover the substrate, also the observable small grains confirm the nanostructural nature of $Cu_2Zn_{0.8}Cd_{0.2}SnS_4$. While, Fig. 2 (c) and (d) show the spherical grains with voids and pores. It was also discovered that the grain size and the density of $Cu_2Zn_{0.8}Cd_{0.2}SnS_4$ nanostructures increase with

increasing of Cu concentration from 0.3 to 0.9 mol/L, which is consistent with the previous reports on copper variation in spray deposited CZTS films [30,31]. It has also been agreed that the conversion efficiency of polycrystalline solar cells increases with the increase of the grain size in the absorber materials; therefore, larger grain size brings advantage to improve the photovoltaics performances [32].
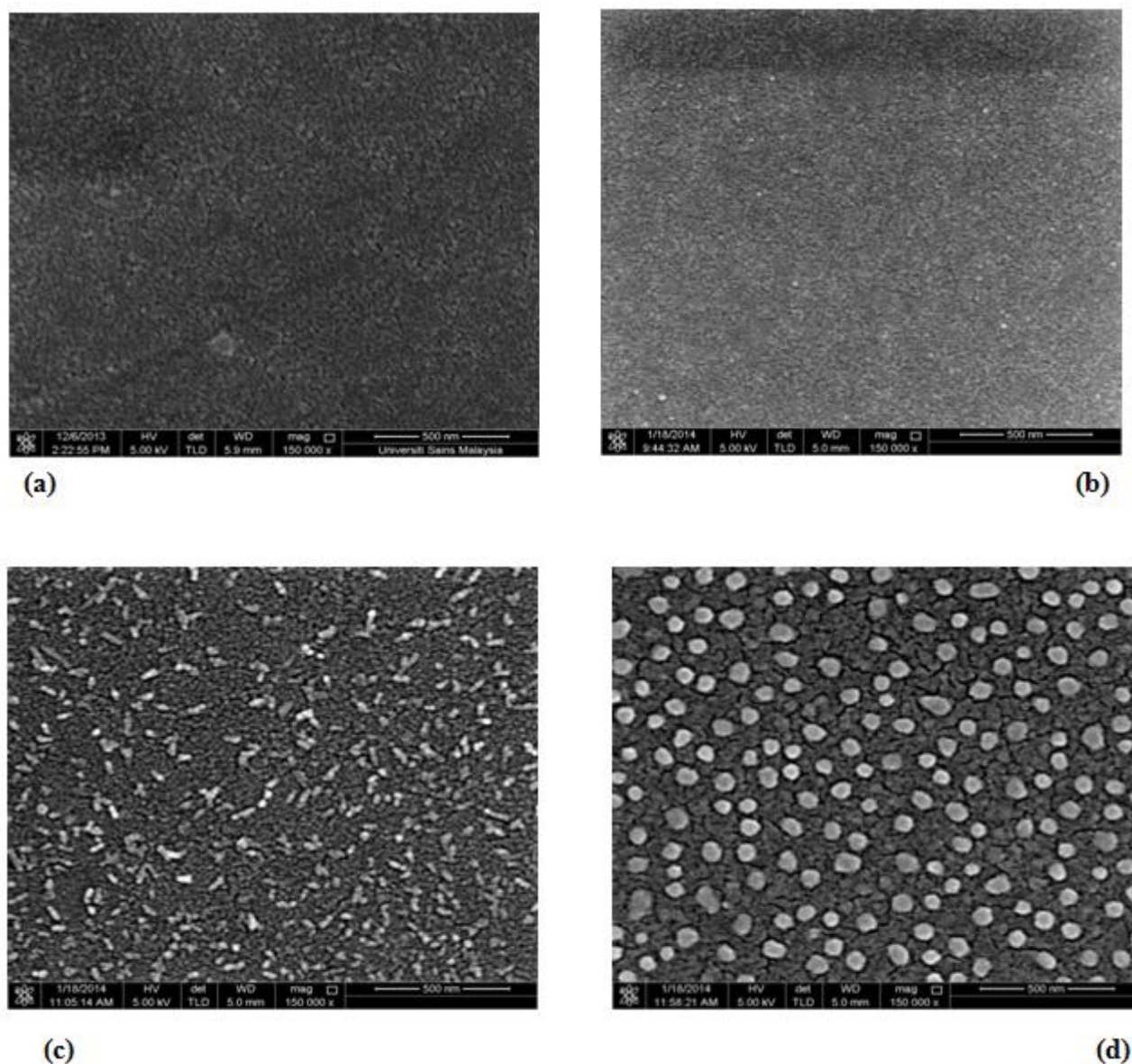

Figure 2. FE-SEM images of $Cu_2Zn_{0.8}Cd_{0.2}SnS_4$ quinternary alloy nanostructures for different Cu concentrations (a) 0.3, (b) 0.5, (c) 0.7 and (d) 0.9 Mol/L.

The elemental ratios of the prepared nanostructures are displayed in Fig. 3.The nanostructures were copper-poor and zinc-rich at 0.3, 0.5 mol/L but increasing Cu and Sn ratio as Cu concentration increases (0.7, 0.9 mol/L). This reveals that the amount of Zn in the $Cu_2Zn_{0.8}Cd_{0.2}SnS_4$ is decreased with increasing Cu ratio. This reduction in Zn amounts may be attributed to evaporation, because the $Cu_2Zn_{0.8}Cd_{0.2}SnS_4$ nanostructures did not contain secondary phases [6].

0.3 mol/L

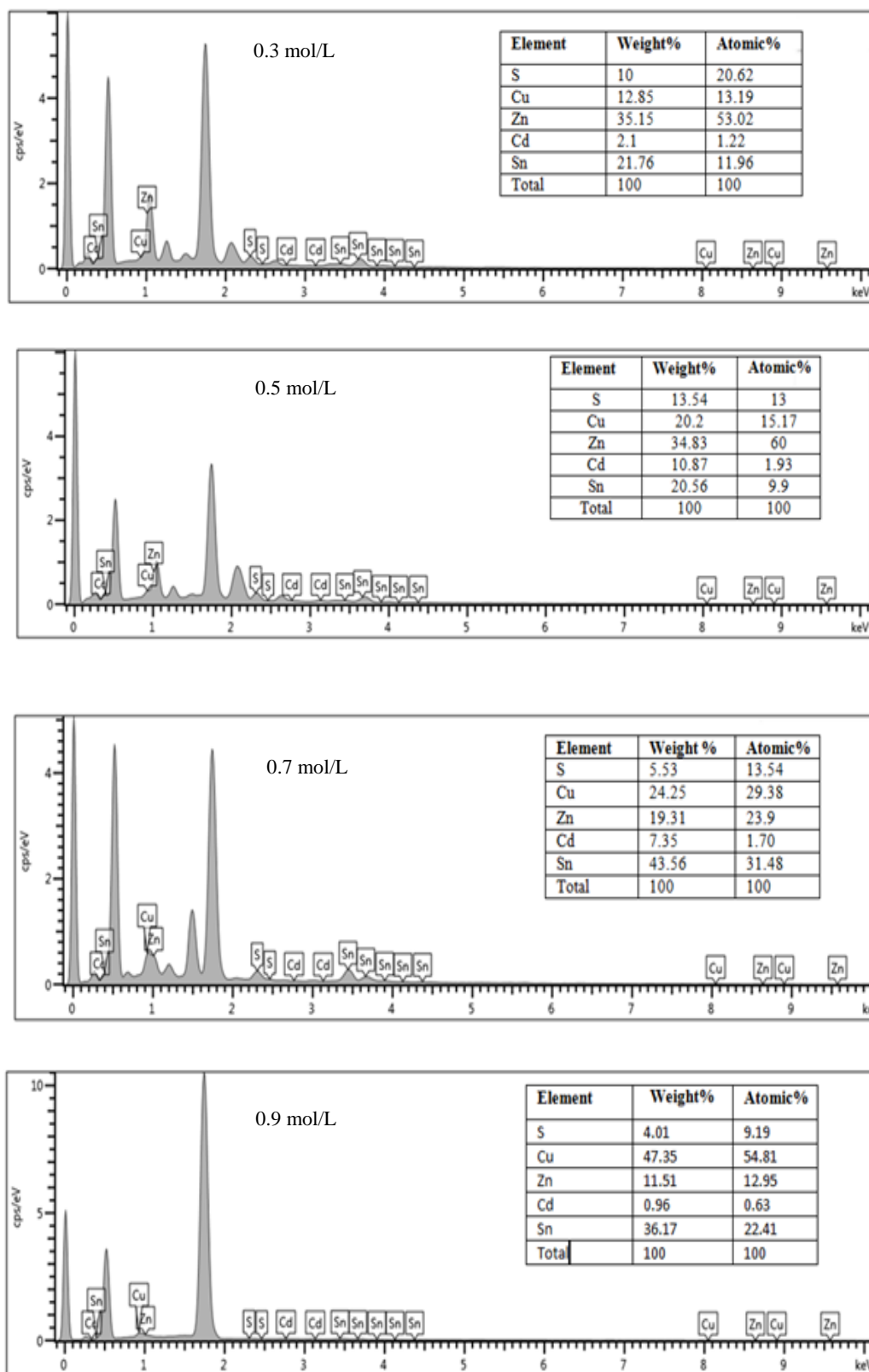| Element	Weight%	Atomic%
S	10	20.62
Cu	12.85	13.19
Zn	35.15	53.02
Cd	2.1	1.22
Sn	21.76	11.96
Total	100	100

0.5 mol/L

Element	Weight%	Atomic%
S	13.54	13
Cu	20.2	15.17
Zn	34.83	60
Cd	10.87	1.93
Sn	20.56	9.9
Total	100	100

0.7 mol/L

Element	Weight %	Atomic%
S	5.53	13.54
Cu	24.25	29.38
Zn	19.31	23.9
Cd	7.35	1.70
Sn	43.56	31.48
Total	100	100

0.9 mol/L

Element	Weight%	Atomic%
S	4.01	9.19
Cu	47.35	54.81
Zn	11.51	12.95
Cd	0.96	0.63
Sn	36.17	22.41
Total	100	100

Figure 3. EDX of $Cu_2Zn_{0.8}Cd_{0.2}SnS_4$ quinternary alloy nanostructures at different Cu concentrations 0.3, 0.5, 0.7 and 0.9 mol/L.

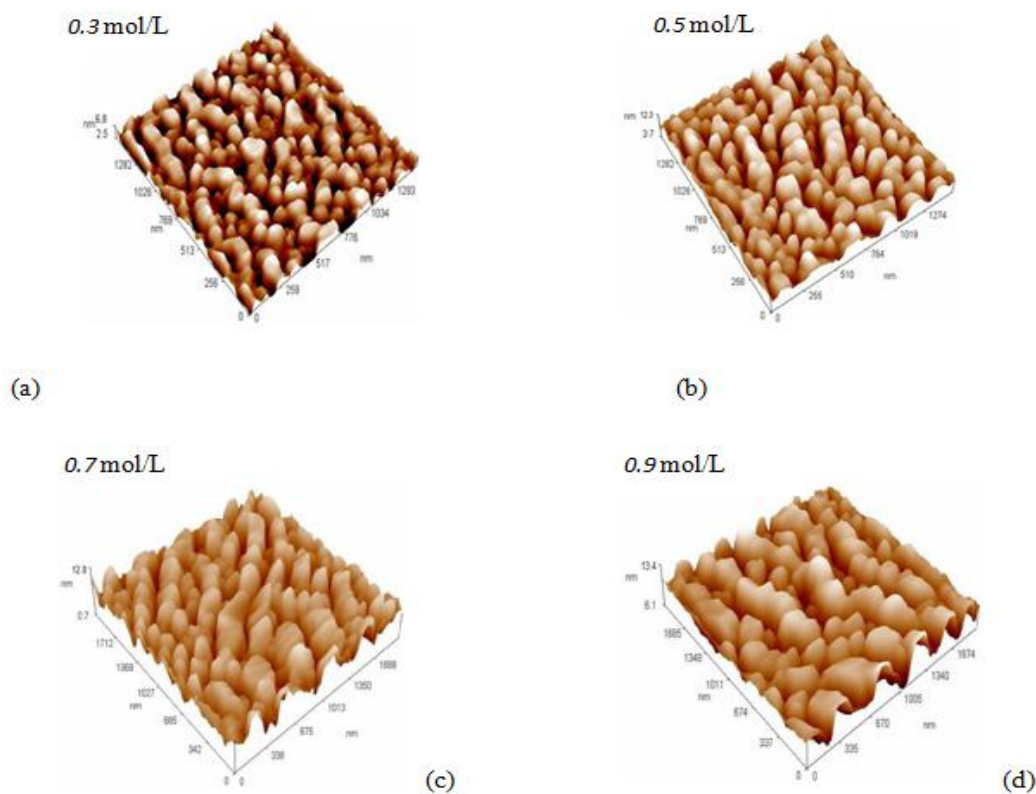**Figure 4.** 3D-AFM images of $Cu_2Zn_{0.8}Cd_{0.2}SnS_4$ nanocrystals for different Cu concentrations (a) 0.3, (b) 0.5, (c) 0.7 and (d) 0.9 Mol/L.

The morphology of $Cu_2Zn_{0.8}Cd_{0.2}SnS_4$ quinternary alloy nanostructures different Cu molarities, was also characterized using AFM. The 3D-AFM images (Figure 4) show a smooth surface with good adherence to the substrate and narrow particles size distribution. The images also demonstrate an increase in surface roughness as Cu concentration increases (Table 2).

The results show an increase in surface quality of $Cu_2Cd_{0.8}Zn_{0.2}SnS_4$ nanocrystals with increasing molar concentration of Cu-precursor. The average particles size calculated from AFM images, was discovered to be higher than estimated by XRD, as given in Table 2.
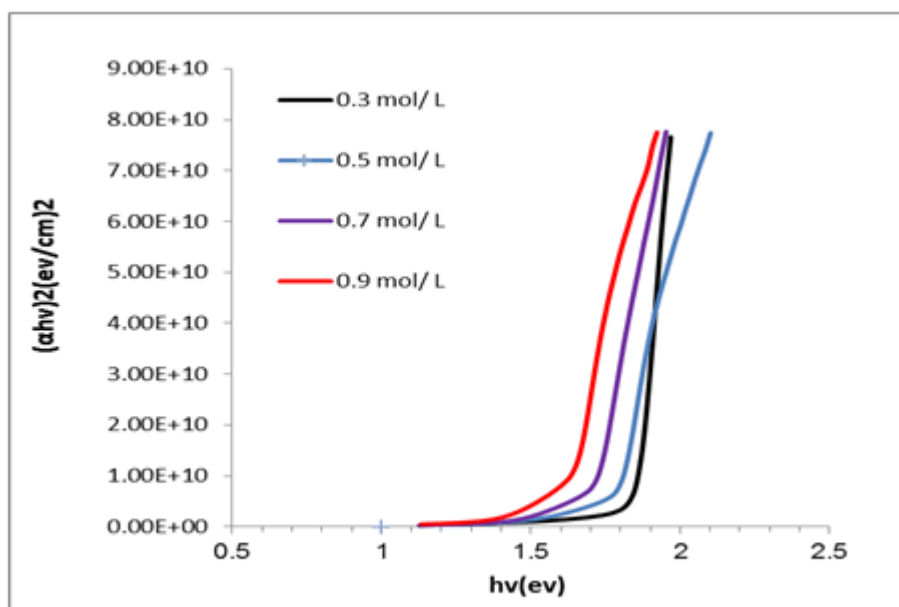
Table 2. Average grain size, roughness of $Cu_2Zn_{0.8}Cd_{0.2}SnS_4$ quinternary alloy nanostructures from AFM.

Molar concentration (mol/L)	Grain size (nm)	Roughness (nm)
0.3	51.92	0.318
0.5	58.60	1.34
0.7	65.56	1.43
0.9	76.43	1.63

3.2 Optical properties
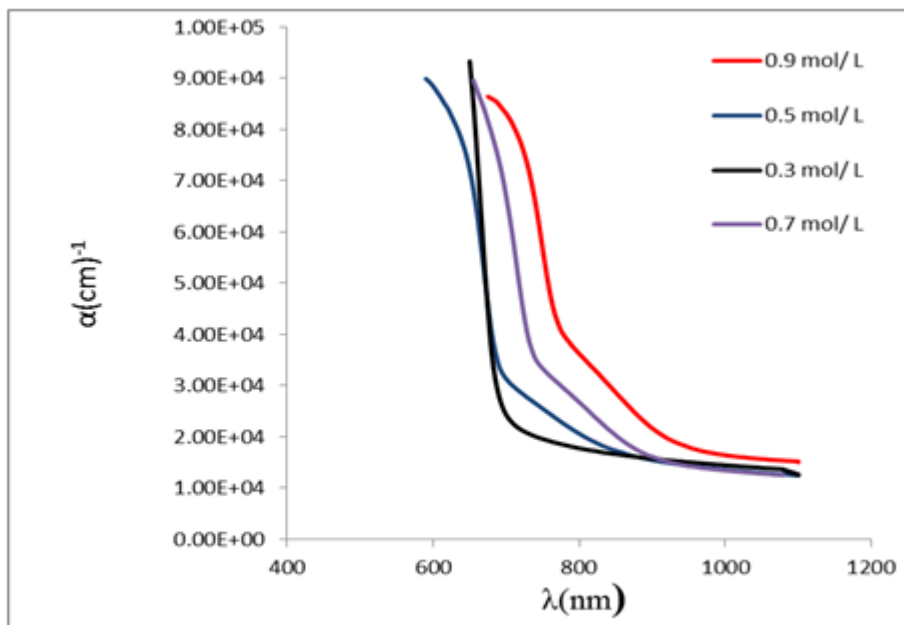
(a)

(b)

Figure 5. Optical properties of $Cu_2Zn_{0.8}Cd_{0.2}SnS_4$ quinternary alloy nanostructure for different Cu concentrations 0.3, 0.5, 0.7 and 0.9 Mol/L (a) The absorption coefficient (b) Absorbance versus photon energy.

The absorbance (A) and the film thickness (t) are utilized for calculating the absorption coefficient associated with the high absorption region, using the relation:

$$\alpha = 2.303 \frac{A}{t}$$

(8)

Figure 5 shows the absorption coefficient (α) of $Cu_2Zn_{0.8}Cd_{0.2}SnS_4$ quinternary alloy nanostructures deposited at different molarity copper 0.3, 0.5, 0.7 and 0.9 mol/L. It was observed that the absorption coefficient is greater than 10^4 cm^{-1}.

Thus, the grown nanostructures were found to exhibit good absorbance in the visible region, also the shifting of absorption spectra toward longer wavelengths was observed with increasing Cu concentration. The fundamental absorption of the material corresponding to the transition from valence to conduction band can be used to determine the band gap. The energy band gap (E_g) is estimated by using the following equation:

$$\left(h\upsilon\alpha\right)^{\gamma} = \beta\left(h\upsilon - E_g\right)$$

(9)

where $h\upsilon$ is the incident photon energy, β is parameter, γ is index characterizes and the optical absorption process equals 2 or 1/2 for indirect and direct transitions, respectively. For direct transition, the best linear fit was obtained for $\gamma = 1/2$. E_g, which is determined by extrapolating the straight line portion $(h\upsilon\alpha)^{\gamma} = 0$ value, ~~and~~ shows a decrease i.e., 1.80 eV, 1.76 eV, 1.68 eV and 1.60 eV for 0.3 M, 0.5 M 0.7 M 0.9 M, respectively (Figure 5). It is found that the energy band gap of $Cu_2Zn_{0.8}Cd_{0.2}SnS_4$ quinternary alloy nanostructures shifts to lower energy with an increase in copper concentration. This shift can be related to the formation of Cu_2S, as shown in the XRD result, characterized by an absorption onset at 1.114 eV. These band gap values are close to the theoretical optimal value required for a single junction solar cell, the CZCTS quinternary alloy nanostructures are appropriate to use as an absorber layer for SCs. Table 3 summarizes the variation of optical band gap with different copper molarity.

Table 3. Optical band gap corresponds to refractive index and optical dielectric constant using Ravindra et al. [33], Herve and Vandamme [34], and Ghosh et al. [35] models of $Cu_2Zn_{0.8}Cd_{0.2}SnS_4$ quinternary alloy nanostructures deposited at different mol/L.

Molar concentration (mol/L)	E_g (eV)	n	ε_∞
0.3	1.8	2.93[a] 2.80[b] 2.68[c]	8.58[a] 7.84[b] 7.18[c]
0.5	1.76	2.95[a] 2.81[b] 2.70[c]	8.70[a] 7.89[b] 7.29[c]
0.7	1.68	3.00[a] 2.85[b] 2.72[c]	9.00[a] 8.12[b] 7.39[c]
0.9	1.60	3.05[a] 2.89[b] 2.75[c]	9.30[a] 8.35[b] 7.56[c]

[a]Ref. [33]; [b]Ref. [34]; [c]Ref.; [35].

The refractive index n is a significant physical parameter in microscopic atomic interactions. Theoretically, the refractive index related to density, and the local polarizability of these entities are the two different approaches in viewing this subject [32]. Many simple relationships between refractive

index n and the energy gap E_g have been attempted [33-40]. Here, various relationships between n and E_g will be reviewed in order to validate the current work. As suggested by Ravindra et al. [33], the band gap and the high frequency refractive index, presented a linear relationship:

$$n = \alpha + \beta \, E_g, \qquad (10)$$

where $\alpha = 4.048$ and $\beta = -0.62$ eV^{-1}.

Inspired by simple physics of light refraction and dispersion, Herve and Vandamme [34] ~~had~~ proposed an empirical relation as:

$$n = \sqrt{1 + \left(\frac{A}{E_g + B} \right)^2} \qquad (11)$$

where $A = 13.6$ eV and $B = 3.4$ eV.

Ghosh et al. [35] had taken a different approach by considering the band structural and quantum-dielectric formulations of Penn [41] and Van Vechten [42]. Introducing, A (contribution from the valence electrons) and B (constant additive to the lowest band gap E_g), the expression was written as:

$$n^2 - 1 = A / (E_g + B)^2, \qquad (12)$$

where $A = 25E_g + 212$, $B = 0.21E_g + 4.25$ and $(E_g + B)$ refers to an appropriate average energy gap of the material.

Thus, these three models for variation of n with energy gap have been tried. Also, the calculated values of the optical dielectric constant (ε_∞) were obtained using the relation $\varepsilon_\infty = n^2$ [43]. The calculated refractive index and optical dielectric constant are as given in Table 3. This is ~~giving~~ showing that the Ghosh model is an appropriate model for solar cells applications.
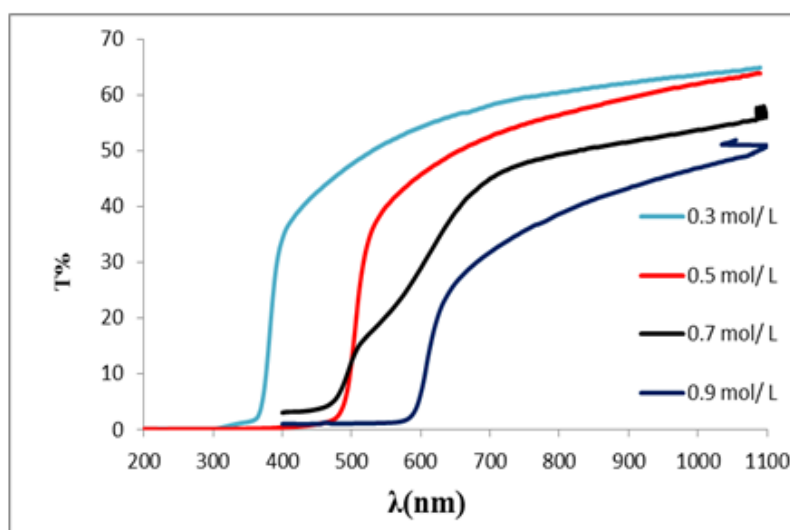

Figure 6. Transmittance spectra of $Cu_2Zn_{0.8}Cd_{0.2}SnS_4$ quinternary alloy nanostructures for different Cu concentrations 0.3, 0.5, 0.7 and 0.9 Mol/L.

Figure 6 shows the transmittance spectra of $Cu_2Zn_{0.8}Cd_{0.2}SnS_4$ quinternary alloy nanostructures at different Cu concentration; i.e. 0.3, 0.5, 0.7 and 0.9 mol/L. All samples have lower transmittance in

the range 63-49%, depending on the Cu concentration. The transmittance is found to be decreased with increasing Cu concentration, may be due to the different thicknesses and roughnesses of nanostructures.

3.3 Electrical characterization

Table 4. Electrical characteristics of $Cu_2Zn_{0.8}Cd_{0.2}SnS_4$ quinternary alloy nanostructures at different Cu concentration; 0.3, 0.5, 0.7 and 0.9 mol/L.

Samples with different Cu concentration (M)	Type of conductivity	Hall coefficient (RH) (m²/C)	Mobility (μ) (cm²/V.s) × 10²	Carrier concentration (cm⁻³)	Resistivity (Ω.cm)
0.3	p-type	3.59×10^6	1.13	7.819×10^{12}	6.3×10^{-1}
0.5	p-type	1.47×10^7	7.76	1.189×10^{13}	4.6×10^{-2}
0.7	p-type	1.65×10^3	8.99	2.419×10^{13}	3.5×10^{-2}
0.9	p-type	1.80×10^5	10.33	3.76×0^{14}	1.45×10^{-2}

The electrical properties of the $Cu_2Zn_{0.8}Cd_{0.2}SnS_4$ quinternary alloy nanostructures at different Cu concentration; 0.3, 0.5, 0.7 and 0.9 mol/L are investigated and given in Table 4. All of the nanostructures showed p-type conduction behavior. The measured resistivity is decreased from 6.3×10^{-1} to 1.45×10^{-2} Ω.cm, with increasing Cu concentration, indicating that the Cu-rich and Sn-rich powders have the lowest grain resistance [44]. Their Hall coefficients ranged from 1.65×10^3 to 1.80×10^5 m²/C and their hole carrier concentrations ranged from 7.819×10^{12} to 3.76×10^{14} cm⁻³. The electrical properties of $Cu_2Zn_{0.8}Cd_{0.2}SnS_4$ quinternary alloy nanostructures at different Cu concentration; 0.3, 0.5, 0.7 and 0.9 mol/L were attributed to the enhanced grain size. The grain boundary decreases as the grain size increases. Thus, effectively reducing the recombination of charge carriers [45,46]. It is clear that the values oscillate ($1.13 \times 10^2 - 10.33 \times 10^2$ cm²/V.s) as Cu concentration increases.

4. CONCLUSION

The spin coating technique proves the feasibility to prepare $Cu_2Zn_{0.8}Cd_{0.2}SnS_4$ quinternary alloy nanostructures. The morphological studies via FE-SEM and AFM prove smooth surfaces and good adherence for photovoltaics and optoelectronics. It is found that the average particle size of $Cu_2Zn_{0.8}Cd_{0.2}SnS_4$ quinternary alloy nanostructure is 35 to 68 nm. The lattice constants are depending on Cu concentration. CZCTS's stiffness depends directly on Cu concentration. In the sample prepared with different copper concentrations, good atomic stoichiometry of the compound was obtained. The elemental composition was close to the stoichiometry of the $Cu_2Zn_{0.8}Cd_{0.2}SnS_4$ quinternary alloy nanostructures. The measured band gap varies from 1.80 to 1.60 eV as Cu increases.

As Cu increases indicating a red shift, the optical band gap decreases. It was confirmed by the structural analysis that the deposited nanostructures are polycrystalline of kesterite (tetragonal) crystal structure. The increasing of particle size when Cu concentration increases was observed, which means

that an enhancement of the particle growth under Cu-rich conditions is observable, where Cu_2S is noticed at 45.70^{o}. As Cu concentration increases, the transmittance decreases as well, and that gave the preference for absorber layer fabrication. After the calculation of refractive index and optical dielectric constant, Ghosh et al. model is recommended for solar cell application. The electrical properties are enhanced as grain size increases.

References

1. K. Ramanathan, G. Teeter, J. C. Keane, R. Noufi, *Thin Solid Films* 480-481, (2005) 499–502
2. S.S. Schmidt, D. Abou-Ras, S. Sadewasser, W. Yin, C. Feng, Y. Yan, *Phys. Rev. Lett.,* 109 (2012) 095506.
3. A. H. Reshak, K. Nouneh, V. Kityk, J. Bila, S. Auluck, H. Kamarudin, Z. Sekkat, *Int. J. Electrochem. Sci.,* 9 (2014) 955.
4. H. Matsushita, T. Maeda, A. Katsui, T. Takizawa, *J. Crys. Growth*, 208 (2000) 416.
5. K. Moriya, J. Watabe, K. Tanaka, H. Uchiki, *phys. stat. sol.* (c), 8 (2006) 2848.
6. A.V. Moholkar, S.S. Shinde, A.R. Babar, K.U. Sim, H.K. Lee, K.Y. Rajpure, et al, *J. Alloys Compound,* 509 (2011) 7439.
7. B.A. Schubert, B. Marsen, S. Cinque, T. Unold, R. Klenk, S. Schorr, et al, *Research and Applications,* 19 (2011) 93.
8. K. Tanaka, T. Shinji, H. Uchiki, *Solar Energy Materials and Solar Cells,* 126 (2014) 143.
9. J. Wang, S. Li, J. Cai, B. Shen, Y. Ren, G. Qin , *J. Alloys and Compound,* 552 (2013) 418.
10. K. Wang, O. Gunawan, T. Todorov, B. Shin, S. J. Chey, N. A. Bojarczuk, D. Mitzi, S. Guha, *Applied Physics Lett.,* 97 (2010) 143508.
11. A. Ennaoui, M. Lux-Steiner, A. Weber, D. Abou-Ras, I. Kötschau, H.-W. Schock, R. Schurr, A. Hölzing, S. Jost, R. Hock, T. Voß, J. Schulze, A. Kirbs, *Thin Solid Films,* 517 (2009) 2511.
12. J. J. Scragga, D. M. Bergb, P. J. Daleb, *Journal of Electroanalytical Chemistry*, 646 (2010) 52.
13. N. Kamoun, H. Bouzouita, B. Rezig, *Thin Solid Films,* 515 (2007) 5949.
14. J. Li, Q. Du, W. Liu, G. Jiang, X. Feng, W. Zhang, J. Zhu, C. Zhu, *Electronic Materials Lett.* 8 (2012) 365.
15. U. Chalapathi, S. Uthanna, V. S. Raja, *Solar Energy Materials and Solar Cells,* 132 (2015) 476.
16. U. Dasgupta, S. K. Saha, A. J. Pal, *Solar Energy Materials and Solar Cells,* 124 (2014) 79.
17. W. Huang, Qi Li, Y. Chen, Y. Xia, H. Huang, C. Dun, Y. Li, D. L. Carroll, *Solar Energy Materials and Solar Cells,* 127 (2014) 188.
18. Y. Al-Douri, Q. Khasawneh, S. Kiwan, U. Hashim, S.B. Abd Hamid, A.H. Reshak, A. Bouhemadou, M. Ameri, R. Khenata, *Energy Convers. Manag*., 82 (2014) 238.
19. A. M. Sherry, M. Kumar, *J. Phys. Chem. Solids,* 52 (1991) 1145.
20. J. L. Tallon, *J. Phys. Chem. Solids,* 41 (1980) 837.
21. M. Kumar, S.P. Upadhyaya, *Phys. Stat. Sol*., (b) 181 (1994) 55.
22. M. Kumar, *Physica B*., 205 (1995) 175.
23. R. K. Pandey, *J. Phys. Chem. Solids*., 59 (1998) 1157.
24. Q. He, Z-T. Yan, *Phys. Stat. Sol.*, (b) 223 (2001) 767-771

25. J. C. Phillips, *Bands and bonds in semiconductors*, Academic Press, San Diego (1973)
26. W. A. Harison, *Electronic structure and properties of solids*, General Publishing Company, Toronto (1989)
27. M. L. Cohen, *Phys. Rev. B*., 32 (1985) 7988.
28. P. K. Lam, M.L. Cohen, G. Martinez, *Phys. Rev. B*., 35 (1987) 9190.
29. Y. Al-Douri, H. Abid, H. Aourag, *Mater. Chem. Phys*., 87 (2004) 14.
30. Y.B. K. Kumar, P. U. Bhaskar, G. S. Babu, V. S. Raja, *phys. stat. sol*., (a) 207 (2010) 149.
31. S.M. Pawar , A.V. Moholkar, I.K. Kim, S.W. Shin, J.H. Moona, J.I. Rhee , J.H. Kim, *Current Applied Physics,* 10 (2010) 565.
32. N. M. Balzaretti, J. A. H. da Jornad, *Solid State Commun.,* 99 (1996) 943.
33. N. M. Ravindra, S. Auluck, V. K. Srivastava, *phys. stat. Sol.,* (b) 93 (1979) k155.
34. P. J. L. Herve, L. K. J. Vandamme, *J. Applied Phys.,* 77 (1995) 5476.
35. D. K. Ghosh, L. K. Samanta, G. C. Bhar, *Infrared Phys.* 24 (1984) 43.
36. Y. Al-Douri, H. Khachai, R. Khenata, Chalcogenides-based quantum dots: Optical investigation using first-principles calculations, Materials Science in Semiconductor Processing 39 (2015) 276–282
37. Y. Al-Douri, U. Hashim, R. Khenata, A.H. Reshak, M. Ameri, A. Bouhemadou, A. Rahim Ruslinda, M.K. Md Arshad, Ab initio method of optical investigations of $CdS_{1-x}Te_x$ alloys under quantum dots diameter effect, Solar Energy 115 (2015) 33–39
38. Y. Al-Douri, *Materials Chemistry and Physics,* 82 (2003) 49.
39. Y. Al-Douri, Y. P. Feng., A. C. H. Huan, *Solid State Commun.,* 148 (2008) 521.
40. Y. Al-Douri, A. H. Reshak, H. Baaziz, Z. Charifi, R. Khenata, S. Ahmad, U. Hashim, An ab initio study of the electronic structure and optical properties of $CdS_{1-x}Te_x$ alloys, Solar Energy 84 (2010) 1979-1984.
41. D. R. Penn, *Physical Review,* 128 (1962) 2093.
42. J. A. Van Vechten, *Physical Review,* 182 (1969) 891.
43. G. A. Samara, *Physical Review B*., 27 (1983) 3494.
44. T. Prabhakar, N. Jampana, *Solar Energy Materials & Solar Cells,* 95 (2011) 1001.
45. T. Tanaka, A. Yoshida, D.Saiki, K.Saito, Q. Guo, M. Nishio, *Thin Solid Films,* 518 (2010) S29.
46. E.M. Mkawi, K. Ibrahim, M. K. M. Ali, A. S. Mohamed, *Int. J. Electrochem. Sci*., 8 (2013) 359.